View Article Online / Journal Homepage / Table of Contents for this issue
Dynamic Article Links

Journal of Materials Chemistry

Cite this: *J. Mater. Chem.*, 2012, **22**, 15128

www.rsc.org/materials

PAPER

Published on 28 May 2012. Downloaded by HK University of Science and Technology on 24/04/2014 05:13:22.

Aggregation-induced red-NIR emission organic nanoparticles as effective and photostable fluorescent probes for bioimaging†

Qiuli Zhao,‡[a] Kai Li,‡[cd] Sijie Chen,[b] Anjun Qin,[a] Dan Ding,[c] Shuang Zhang,[a] Yi Liu,[a] Bin Liu,*[cd] Jing Zhi Sun*[a] and Ben Zhong Tang*[abd]

Received 5th March 2012, Accepted 22nd May 2012
DOI: 10.1039/c2jm31368e

Organic fluorescent probes are widely used in bioimaging and bioassays, but the notorious photobleaching hampers their applications. Encapsulation of organic dyes into nanoparticles (NPs) is an effective strategy to minimize photobleaching, but classical organic dye molecules tend to have their fluorescence quenched in aggregate states, which is termed aggregation-caused quenching (ACQ). Here we demonstrate our attempt to tackle this problem through the aggregation-induced emission (AIE) strategy. 3,4:9,10-Tetracarboxylic perylene bisimide (PBI) is a well-known organic dye with a serious ACQ problem. By attaching two tetraphenylethene (TPE) moieties to the 1,7-positions, the ACQ-characteristic PBI-derivative was converted to an AIE-characteristic molecule. The obtained PBI derivative (BTPEPBI) exhibits several advantages over classical PBI derivatives, including pronounced fluorescence enhancement in aggregate state, red to near infrared emission, and facile fabrication into uniform NPs. Studies on the staining of MCF-7 breast cancer cells and *in vivo* imaging of a tumor-bearing mouse model with BTPEPBI-containing NPs reveal that they are effective fluorescent probes for cancer cell and *in vivo* tumor diagnosis with high specificity, high photostability and good fluorescence contrast.

Introduction

Fluorescent probes based on organic dyes have proven to be powerful tools in modern bioimaging.[1,2] In both fundamental investigation and practical application, red to near infrared (red-NIR) fluorescent dyes with high stability are in demand, because the red-NIR emission allows the probing molecules to be excited with a visible light source, which results in less harmful effects on the biological samples such as cells and tissues in comparison with ultraviolet (UV) light. Meanwhile, the longer excitation and emission wavelength enables the light to penetrate through thicker samples which is beneficial to *in vivo* experiments.[3] High stability permits the imaging process to last for a long period with attenuated photobleaching, thereby allowing more information to be derived about biological events. In this aspect, employing inorganic quantum dots (QDs) as fluorescent probes is a helpful strategy to get desirable stability.[4] However, some side effects (*e.g.* hazardous heavy metal species) have to be clearly addressed and elucidated before they could be successfully used for *in vivo* imaging applications.

It is a rational strategy to encapsulate organic red-NIR emission dyes into nanoparticles (NPs) with biocompatible shells, similar to the strategy widely used in the preparation of fluorescent QDs. However, to yield high quality fluorescent NPs, some critical criteria must be satisfied concurrently. Firstly, the red-NIR emission dyes should have desirable photochemical stability. And secondly, the red-NIR dyes should have desirable fluorescence quantum efficiency (Φ_F) when they are encapsulated into NPs. Perylene-3,4:9,10-tetracarboxylic bisimide (PBI) derivatives have shown remarkable thermal and photochemical stability and high Φ_F values in solutions.[5] In addition, some PBIs emitted red fluorescence in solid states.[6] Moreover, they have been widely used as active materials in organic solar cells, acceptor-based molecular electronics, and fluorescent biosensors.[7–9] However, it is a great challenge to make the NPs of PBIs highly emissive. Although PBIs usually demonstrate near-unity Φ_F values in dilute solutions;[5] in poor solvents or in solid states, PBI molecules are prone to form aggregates, which lead to

[a]*MOE Key Laboratory of Macromolecular Synthesis and Functional-ization, Institute of Biomedical Macromolecules, Department of Polymer Science and Engineering, Zhejiang University, Hangzhou 310027, China. E-mail: sunjz@zju.edu.cn; Fax: +86-571-87953734*
[b]*Department of Chemistry, Institute for Advanced Study, State Key Laboratory of Molecular NeuroScience, and Division of Biomedical Engineering, The Hong Kong University of Science & Technology, Clear Water Bay, Kowloon, Hong Kong, China. E-mail: tangbenz@ust.hk; Fax: +86-852-2358-7375*
[c]*Department of Chemical & Biomolecular Engineering, National University of Singapore, Singapore, 117576, Singapore. E-mail: cheliub@nus.edu.sg*
[d]*Institute of Materials Research and Engineering, 3 Research Link, 117602, Singapore*

† Electronic supplementary information (ESI) available. See DOI: 10.1039/c2jm31368e

‡ Miss Qiuli Zhao and Dr Kai Li contributed equally to this work.

This journal is © The Royal Society of Chemistry 2012

View Article Online

Published on 28 May 2012. Downloaded by HK University of Science and Technology on 24/04/2014 05:13:22.

fluorescence (FL) quenching due to effective intermolecular π–π stacking in the aggregates.[5,6,10] Such a phenomenon is more serious for red-NIR dyes because the long wavelength emission is often achieved by extending the conjugation of the fluorescent cores, which favors intermolecular π–π interaction and intermolecular packing. To sustain efficient emission in the solid states, bulky substituents are attached onto PBIs to hinder the intermolecular π–π stacking and molecular aggregation.[10b,11]

Tetraphenylethene (TPE), a propeller-shaped conjugated molecule was reported to show an unusual fluorescent behavior. It is non-emissive in solution but highly emissive in aggregate form. This phenomenon is given the term "aggregation-induced emission" (AIE).[12] Recently, we have demonstrated that the conjugation of TPE moieties with classical fluorogens such as naphthalene, anthracene, quinoline, triphenylamine and pyrene could yield new dyes as efficient emitters in aggregates or in solid films.[13]

However, all these dyes are blue or green emitters, which are not ideal for imaging applications. To further develop red-NIR emitters with AIE characteristics, in the present work, we attached two TPE moieties to the 1,7-positions on perylene 3,4:9,10-tetracarboxylic bisimide core *via* ether linkages (Chart 1, BTPEPBI). Conjugation of two TPE moieties to the PBI core was also found to red-shift the emission, leading to a PBI-based red-NIR fluorogen. Further encapsulation of the red-NIR fluorogen with polymer matrix led to folic acid functionalized NPs, which showed great promise for both *in vitro* and *in vivo* imaging applications.

Results and discussion

Synthesis of BTPEPBI

The synthetic routes to the intermediates and the final product BTPEPBI are shown in Schemes 1 and 2, and the detailed procedures for the syntheses of these compounds are described in the Experimental section and ESI.† In brief, bromination of perylene-3,4:9,10-tetracarboxylic dianhydride was conducted according to ref. 14 to yield a mixture of 1,6-dibromo-3,4:9,10-perylene tetracarboxylic dianhydride (1,6-DBrPTCDA) and 1,7-dibromo-3,4:9,10-perylene tetracarboxylic dianhydride (1,7-DBrPTCDA). As the separation of these two isomers was reported to be difficult, we proceeded to the imidization reaction without purification. The reaction afforded a mixture of *N*,*N*′-dicyclohexyl-1,7-dibromoperylene-3,4:9,10-tetracarboxylic bisimide (1,7-DBrPBI) and its isomer *N*,*N*′-dicyclohexyl-1,6-dibromoperylene-3,4:9,10-tetracarboxylic bisimide (1,6-DBrPBI). The other intermediate of 1-(4-hydroxyphenyl)-1,2,2-triphenylethene was prepared by cross-coupling of 4-hydroxyl-phenylbenzophenone and benzophenone using Zn powder as the catalyst (Scheme 1). Coupling between the mixed 1,6-/1,7-DBrPBI and 1-(4-hydroxyphenyl)-1,2,2-triphenylethene was conducted in *N*-methyl-2-pyrrolidone in the presence of K_2CO_3 at 80 °C (Scheme 2) led to a mixture of 1,7-BTPEPBI and 1,6-BTPEPBI. The purification was carried out using simple column chromatography with dichloromethane as the eluent. The yields for 1,7-BTPEPBI and 1,6-BTPEPBI were 64% and 17%, respectively. This procedure is much easier as compared to the previous reports, which represent one of the very few successful examples of isolation and characterization of pure 1,6- and 1,7-disubstituted PBIs.[15] The structures of the intermediates and products were characterized with multiple spectroscopic techniques and satisfactory data are shown in the Experimental section and ESI.† As 1,7-BTPEPBI is the dominant product, it is used for the subsequent studies.

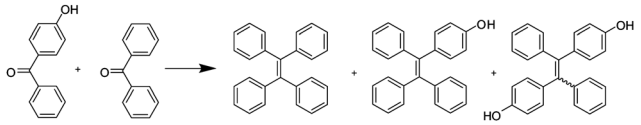

Scheme 1 Synthetic route to 1-(4′-droxylphenyl)-1,2,2-triphenylethene. *Reagents and conditions*: Zn, $TiCl_4$, THF, reflux, N_2, overnight.

Aggregation-induced emission

We studied the FL behavior of BTPEPBI in water–THF mixtures. As shown in Fig. 1A, in dilute THF solution,

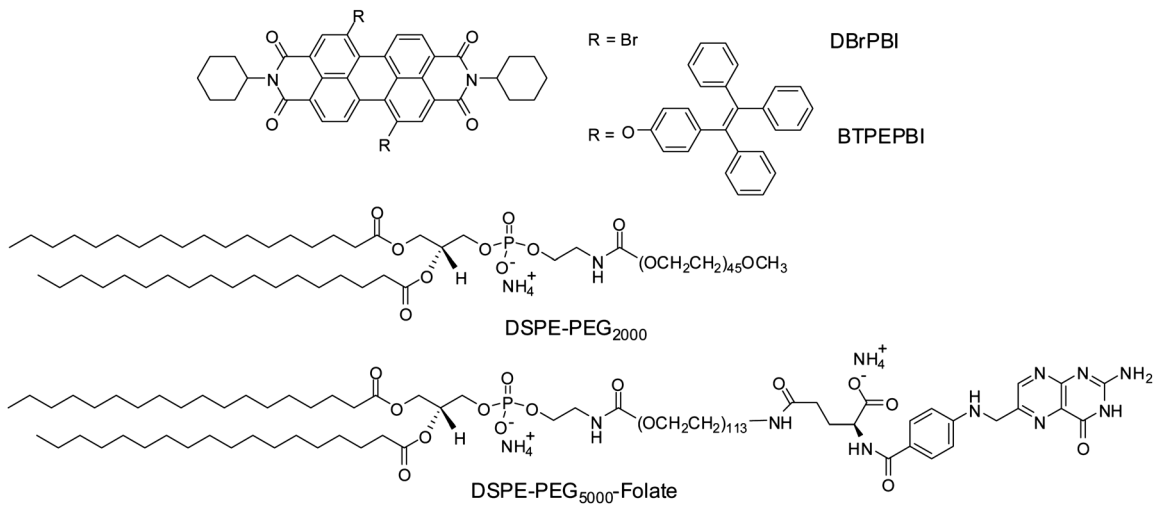

Chart 1 The molecular structures of 1,7-dibromo-substituted PBI (DBrPBI), 1,7-tetraphenylethene modified PBI derivative (BTPEPBI), DSPE–PEG_{2000} and DSPE–PEG_{5000}–folate.

View Article Online

Published on 28 May 2012. Downloaded by HK University of Science and Technology on 24/04/2014 05:13:22.

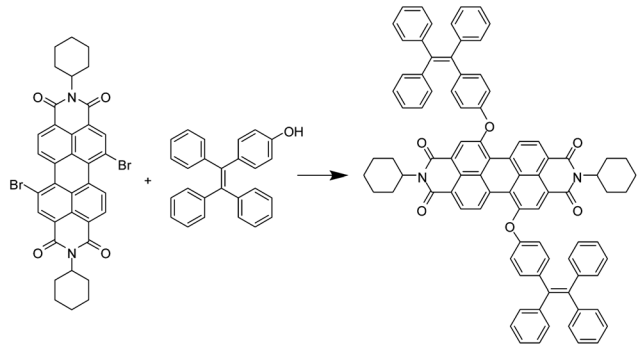

Scheme 2 Synthetic route to BTPEPBI. *Reagents and conditions*: K_2CO_3, NMP, 80 °C, N_2, 24 h.

BTPEPBI shows very weak fluorescence. The Φ_F is only 0.03% using Rhodamine 6G in ethanol as the standard (Fig. S3†). When f_w (volume fraction of water) varies from 0 to 50%, the FL spectra of the solutions have very small changes. When f_w is 50% or higher, both of FL intensity and Φ_F value increase evidently (Fig. 1A and S3†). The enhancements are ascribed to aggregate formation, which are induced by the addition of water. The aggregation process was also monitored with absorption spectra (Fig. S2†). The changes in the absorption features, especially the relative intensity of 0–0 and 0–1 transitions, indicate strong molecular aggregation by π–π stacking. At f_w = 90%, Φ_F is boosted up to 8.0%, which is 267 times the Φ_F for its THF solution. The Φ_F for BTPEPBI solid films is as high as 13%, corresponding to an AIE amplified factor of 433 ($\alpha_{AIE} = \Phi_{F,film}/\Phi_{F,solution}$). In addition, $I/I_0 - 1$ data show that the FL intensity is enhanced over 233 times when f_w changes from 0 to 90% (Fig. 1B). These results indicate that BTPEPBI is a typical AIE molecule. In solutions, the phenyls in the TPE units around the PBI core undergo strong rotations, which exhausts the excited energy and renders it non-emissive. In aggregates, the propeller shape of TPE blocks BTPEPBI molecules packing closely through π–π stacking, while molecular stacking restricts the rotations of phenyls in TPE units. This restriction of intramolecular rotations (RIR) suppresses the non-radiative channel and induces its emission.

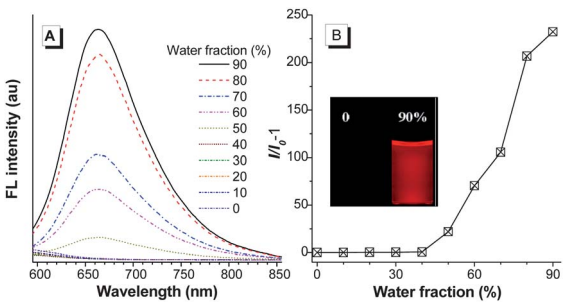

Fig. 1 (A) FL spectra of BTPEPBI in THF–H_2O mixtures with different f_w values, excited at 538 nm. (B) Plot of $I/I_0 - 1$ *vs.* f_w, I and I_0 are the FL intensity of BTPEPBI in THF–H_2O mixtures in the presence and absent of H_2O, respectively. The inset shows the FL photographs of BTPEPBI in pure THF and THF–H_2O mixture (f_w = 90%). [BTPEPBI] = 1×10^{-5} mol L^{-1}.

An important feature of Fig. 1A is that the emission maximum for the BTPEPBI aggregates appears at around 664 nm. The inset in Fig. 1B shows clear red emission from the BTPEPBI aggregates under illumination of UV light (365 nm). Moreover, the FL spectrum ranges from 600 to 850 nm, covering a rather large area in the NIR region. We further evaluated the stability of BTPEPBI by thermal gravimetric analyzer (TGA) and the measurement result revealed that BTPEPBI solid lost 5% of its original weight at the temperature of 247 °C in N_2 atmosphere, indicating high thermal stability (Fig. S4†). The red-NIR emission and desirable Φ_F allow the aggregates of BTPEPBI to be used as potential fluorescent probe for bioimaging.

Nanoparticle preparation

The attachment of bulky and rigid TPE moieties onto PBI core has converted the emission behavior from ACQ to AIE. In many situations, PBI derivatives are prone to form ordered nano- or micro-structures such as wires, ribbons, and rods.[6,16] Scanning electron microscopy (SEM) was used to study the morphology of the aggregates formed in the THF–water mixtures and the images are displayed in Fig. 2. BTPEPBI molecules tend to aggregate into microfibers in a wide f_w range from 30% to 60% (Fig. S5†). A notable characteristic is that the lengths of the fibrils can be several-hundred micrometers or millimeters. In other solvent–non-solvent mixtures, such as dichloromethane–methanol, the trend of microfiber formation has also been observed (Fig. S6†). More importantly, the confocal fluorescence image shows that the microfibers have bright red emission upon excitation by a 488 nm laser (Fig. 2D).

The red emission is desirable for bioimaging, but the microfibers are too large to be practically employed as probes in living cells. Alternatively, we fabricated NPs through a modified nanoprecipitation method,[17] using a mixture of 1,2-distearoyl-*sn*-glycero-3-phosphoethanolamine-*N*-[methoxy(polyethylene glycol)-2000] (DSPE–PEG_{2000}) and DSPE–PEG_{5000}–folate (Chart 1) as the encapsulation matrix to yield NPs with good biocompatibility and different surface folic acid densities. BTPEPBI-NP0 and BTPEPBI-NP50 represent BTPEPBI-based

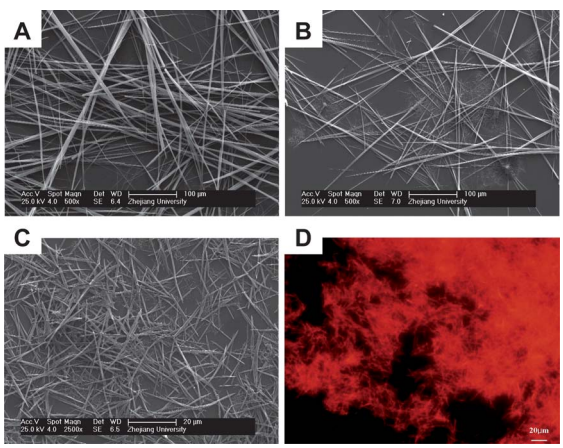

Fig. 2 SEM images of the microfibers formed by BTPEPBI molecules in THF–H_2O mixtures with f_w of 30% (A), 40% (B) and 50% (C), respectively. (D) A confocal FL image of the aggregates in sample (C) (excited at 488 nm).

 This journal is © The Royal Society of Chemistry 2012

View Article Online

Published on 28 May 2012. Downloaded by HK University of Science and Technology on 24/04/2014 05:13:22.

NPs that were formulated with polymers containing the feed ratio of 0% and 50% for DSPE–PEG_{5000}–folate in the polymer matrix. During NP formation, the hydrophobic DSPE segments tend to be embedded into the hydrophobic core while the hydrophilic PEG-folate chains extend into the aqueous phase.

The morphology of BTPEPBI-NP50 was studied by high resolution transmission electron microscopy (HR-TEM, Fig. 3 inset). The spherical shape of BTPEPBI-NP50 can be clearly distinguished from the black dots due to the high electron density of BTPEPBI molecules. Laser light scattering results suggest a narrow particle size distribution for BTPEPBI-NP50 (Fig. 3), and the volume average hydrodynamic diameter of BTPEPBI-NP50 is 57 ± 1 nm. The absorption and FL spectra of BTPEPBI-NP50 in water are depicted in Fig. 4. Both the quantum yield and emission spectrum shape for BTPEPBI-NP50 are similar to those of the nano-aggregates formed in THF–water ($f_w = 90\%$), with the FL maximum for the former slightly red-shifted to 680 nm. As shown in Fig. 4, there is almost no overlap between the absorption and emission spectra of BTPEPBI-NP50 in water, which is beneficial to the confocal FL image.

Cell stain and *in vivo* imaging

MCF-7 breast cancer cells with high folate receptor expression level in cell membrane were chosen to evaluate the targeting ability of BTPEPBI-NP50 over BTPEPBI-NP0.[18] The effect of NPs' surface folic acid on MCF-7 breast cancer cell uptake was studied by confocal laser scanning microscopy. Fig. 5A and B show the recorded images of MCF-7 breast cancer cells after incubation with BTPEPBI-NP0 and BTPEPBI-NP50 suspensions for 2 h in culture medium containing 2 μM BTPEPBI, respectively. The cell nuclei were stained with 4′,6-diamidino-2-phenylindole (DAPI). These images were taken upon excitation at 543 nm with a 560 nm longpass barrier filter.

It should be noted that no auto FL from the cell itself can be detected under the same experimental conditions (Fig. 5C). In addition, the FL intensity from cell cytoplasm after incubation with BTPEPBI-NP50 (Fig. 5B) is higher than that with BTPEPBI-NP0 (Fig. 5A). Quantitative studies using Image-Pro Plus 5.0 software indicate that the average FL intensity of red signal in Fig. 5B is ~1.7 times higher than that in Fig. 5A. The three-dimensional (3D) confocal image of the corresponding cells incubated with BTPEPBI-NP50 shows that the intense FL is mainly from NPs internalized in the MCF-7 cell cytoplasm (Fig. 5D). The higher FL intensity of MCF-7 cancer cells in Fig. 5B as compared to that in Fig. 5A suggests that more NPs

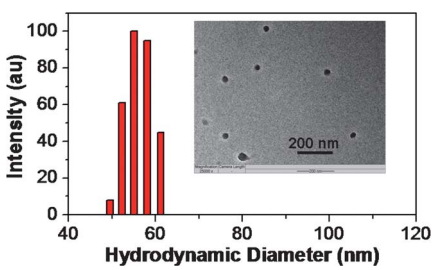

Fig. 3 Particle size distribution of BTPEPBI-NP50 in water studied *via* laser light scattering. Inset: HR-TEM image of BTPEPBI-NP50.

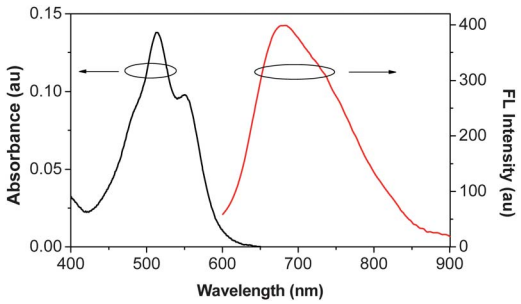

Fig. 4 UV-vis absorption and FL spectra of BTPEPBI-NP50 in water at room temperature (excited at 543 nm).

are internalized into the cells due to specific interactions between folic acid on NP surface and folate receptors in the cancer cell membrane, which should favor folate receptor-mediated endocytosis.[19]

The photostability of the NPs is a crucial parameter for bioimaging because high photostability allows the imaging process to last for a long period with attenuated photobleaching. We evaluated the photostability of BTPEPBI-NP50 by using confocal microscopy and analyzed the intensity using Image-Pro Plus 5.0 software and the data are summarized in Fig. 6. I_0 is the initial fluorescence intensity and I is the fluorescence intensity of the sample after continuous scanning for designated time intervals. It can be seen that the FL intensity decreases steadily without any abrupt quenching. Upon continuous excitation at 543 nm (0.5 mW) for 35 min, only 14% FL intensity loss was recorded. This observation indicates the NPs have good photostability and are promising in bioimaging.

In vivo imaging based on BTPEPBI-NP50 and BTPEPBI-NP0 was studied on a tumor-bearing mouse model. The animal model was established by subcutaneously inoculating murine hepatic H_{22} cancer cells into the left axillary space of each mouse. When the tumor volume reached about 300 mm^3, the mice were

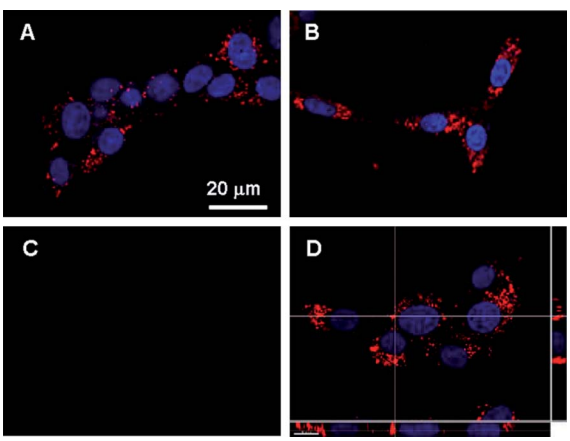

Fig. 5 Confocal images of MCF-7 cancer cells after incubation with (A) BTPEPBI-NP0 and (B) BTPEPBI-NP50 for 2 h at 37 °C ([BTPEPBI] = 2 μM). The FL of BTPEPBI-NPs was recorded under excitation at 543 nm. The blue signal indicates cell nuclei stained by DAPI. (C) Confocal images of the cells without incubation with BTPEPBI-NPs. (D) 3D image of cells incubated with BTPEPBI-NP50 for 2 h at 37 °C. The scale bar is the same for all images.

View Article Online

Published on 28 May 2012. Downloaded by HK University of Science and Technology on 24/04/2014 05:13:22.

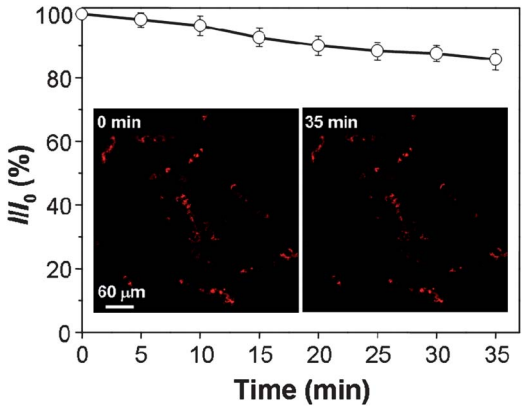

Fig. 6 Photostability of BTPEPBI-NP50 upon continuous excitation at 543 nm for 0 to 35 min (0.5 mW). I_0 is the initial fluorescence intensity and I is the fluorescence intensity of the sample after continuous scanning for designated time interval. The inset shows the corresponding confocal images at 0 and 35 min.

intravenously injected with BTPEPBI-NP50 and BTPEPBI-NP0, respectively. The mice were subsequently imaged by a Maestro EX *in vivo* fluorescence imaging system. Fig. 7A shows the *in vivo* distribution of BTPEPBI-NP0 in the tumor-bearing mouse at 1 and 3 h post-injection. The different FL intensities are shown by different colors, and the order of red, orange, yellow, green, and blue refers to a successive decrease in intensity. Obvious FL is observed in the area of tumor tissue at 1 and 3 h, suggesting that BTPEPBI-NP0 has efficiently accumulated in tumor through enhanced permeability and retention (EPR) effect.[20]

In addition, strong FL from the liver region is also observed, which implies that some NPs in the blood circulation tend to be enriched in the liver. This agrees well with the previous reports that NPs with a size of 50–60 nm have a tendency to undergo reticuloendothelial system (RES) uptake to be enriched in different organs including in the liver.[21] The specific tumor targeting ability of BTPEPBI-NP50 is also evaluated on the same tumor-bearing mouse model, as displayed in Fig. 7B. Much higher FL intensity is shown in the tumor tissue of BTPEPBI-NP50-treated mouse as compared to that of BTPEPBI-NP0-treated mouse at both 1 and 3 h post-injection respectively, demonstrating that BTPEPBI-NP50 has the specific targeting ability to the tumor that contains folate receptor-over expressed cancer cells in a living body. These results illustrate that BTPEPBI-NP50 is an effective fluorescent probe for *in vivo* tumor diagnosis with high specificity and good FL contrast.

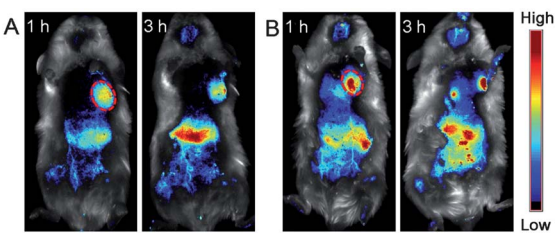

Fig. 7 *In vivo* FL imaging of H_{22} tumor-bearing mice after intravenous injection of BTPEPBI-NP0 (A) and BTPEPBI-NP50 (B), respectively. The red circle indicates the tumor site.

Concluding remarks

In summary, we have successfully derived an AIE active fluorogen (BTPEPBI) by attachment of two TPE moieties on the 1,7-positions of a PBI core. In solvent–nonsolvent mixtures, BTPEPBI molecules are prone to aggregate into microfibrils, which emit red FL with a peak at around 664 nm. The Φ_F values are 13% and 8% for BTPEPBI thin film and BTPEPBI aggregates in the THF–H_2O mixture with f_w of 90%, respectively. The α_{AIE} value is as high as 433. To make use of the aggregates in cell stain and *in vivo* investigations, amphiphilic copolymers DSPE–PEG_{2000} and DSPE–PEG_{5000}–folate have been employed in the fabrication of dye-containing NPs as BTPEPBI-NP0 and BTPEPBI-NP50. The NPs have expected spherical shape with narrow particle size distribution. They are red-NIR fluorescent with an emission peak at around 680 nm and an emission spectrum ranging from 660 to 850 nm.

After incubation with MCF-7 breast cancer cells for 2 h, the confocal images showed that both BTPEPBI-NP0 and BTPEPBI-NP50 were internalized in MCF-7 cell cytoplasm, and BTPEPBI-NP50 had higher loading rate due to specific interactions between folic acid on NP surface and folate receptors in the cancer cell membrane. *In vivo* imaging studies on H_{22} tumor-bearing mouse model using BTPEPBI-NP50 and BTPEPBI-NP0 as fluorescent probes have revealed that the injected NPs are efficiently accumulated in the tumor through EPR effect. In addition, the tumor tissue of BTPEPBI-NP50-treated mouse displays much higher FL intensity in comparison with that of BTPEPBI-NP0-treated mouse, indicating that BTPEPBI-NP50 has specific targeting ability to the tumor that contains folic acid receptor over expressed cancer cells in a living body. More importantly, the fluorescent probe of BTPEPBI-NP50 is effective for *in vivo* tumor diagnosis with high specificity and good FL contrast due to AIE activity of the novel dye. With red-NIR emission, pronounced AIE activity and high photostability, the BTPEPBI-containing NPs may find more applications in both fundamental and practical research on living systems. The organic NPs based on AIE active molecules provide a new strategy to construct very bright and highly photobleaching resistant fluorescent probes.

Experimental

Chemicals and materials

All the chemicals used were purchased from Acros or Alfa, unless specifically stated. 4-Hydroxybenzophenone was purchased from an industrial supplier, and it was recrystallized before usage. Bromine was purchased from Alladin. 1,2-Distearoyl-*sn*-glycero-3-phosphoethanolamine-*N*-[methoxy(poly-ethylene glycol)-2000] (DSPE–PEG_{2000}) was a gift from Lipoid GmbH (Ludwigshafen, Germany). DSPE–PEG_{5000}–folate was a commercial product of Avanti Polar Lipids, Inc. 4′,6-Diamidino-2-phenylindole (DAPI), 3-(4,5-dimethyl-thiazol-2-yl)-2,5-diphenyl tetrazolium bromide (MTT), penicillin–streptomycin solution, and trypsin–EDTA solution were purchased from Sigma-Aldrich. Fetal bovine serum (FBS) was purchased from Gibco (Life Technologies, AG, Switzerland). Milli-Q water was supplie by Milli-Q PlusSystem (Millipore Corporation, Breford, USA). Water was deionized for three times before using. MCF-7 breast

 This journal is © The Royal Society of Chemistry 2012

View Article Online

Published on 28 May 2012. Downloaded by HK University of Science and Technology on 24/04/2014 05:13:22.

cancer cells were provided by American Type Culture Collection. Murine hepatic H_{22} cancer cells were purchased from Shanghai Institute of Cell Biology (Shanghai, China). THF was distilled under nitrogen from sodium benzophenone ketyl immediately prior to use. All other solvents were in analytical grade and were purified using standard methods.

Instrumentations

^{1}H and ^{13}C NMR spectra were measured on a Bruker ARX 300 MHz NMR or 400 MHz NMR spectrometer in $CDCl_3$ or DMSO-d_6 using tetramethylsilane (TMS; $\delta = 0$ ppm) as internal standard. Elemental analysis was performed on a Thermo-Finnigan Flash EA1112 apparatus. FL spectra were recorded on a LS 55 spectrofluorometer (Perkin Elmer, USA). The UV-vis spectra were recorded on a Shimadzu UV-1700 spectrometer, or on a Milton Roy Spectronic 3000 Array spectrophotometer. Fluorescence quantum yields (Φ_F) were estimated using Rhodamine 6G in ethanol as the standard (Φ_F = 95%), the absorbance of the solutions was kept around 0.05 to avoid internal filter effect. The solid state Φ_F was recorded by a calibrated integrating sphere on a Photon Technology International time-resolved fluorescence spectroscopy. The average particle size and size distribution of the NPs were determined by laser light scattering with particle size analyzer (90 Plus, Brookhaven Instruments Co. USA) at a fixed angle of 90° at room temperature. The morphology of the NPs was studied by high-resolution transmission electron microscope (HR-TEM, JEM-2010F, JEOL, Japan). Scanning electron microscope (SEM) images were taken on a JSM-5510 scanning electron microscopy. The FL micrographs were recorded on an inverted fluorescence microscope (Nikon Eclipse TE2000-U). Thermal stabilities were evaluated by measuring TGA thermograms on a TA Instruments TGA Q5000 under nitrogen at a heating rate of 20 °C min^{-1}.

Synthesis

The final BTPEPBI conjugate was synthesized by reaction of its precursor *N*,*N*′-dicyclohexamethyl-1,7-dibromo-3,4:9,10-tetracarboxylic perylene bisimide (DBrPBI) with 1-(4′-hydroxyl-phenyl)-1,2,2-triphenylethene. The DBrPBI was prepared according to ref. 14 and 15. The synthetic routes to 1-(4′-hydroxyl-phenyl)-1,2,2-triphenylethene and target compound are shown in Schemes 1 and 2, respectively. The experimental procedures are given below.

Synthesis of 1-(4-hydroxyphenyl)-1,2,2-triphenylethene

4-Hydroxyl-phenylbenzophenone (1.9 g, 10 mmol), benzophenone (2.2 g, 12 mmol), and Zn powder (2.9 g, 44 mmol) were added to a 250 mL two-necked round-bottom flask. The flask was evacuated under vacuum and flushed with nitrogen three times. Then 80 mL newly dried THF was added. The solution was cooled to 0 °C, into which $TiCl_4$ (2.4 mL, 22 mmol) was added. The mixture was refluxed overnight. After cooling to room temperature, 80 mL dilute hydrochloric acid (1 mol L^{-1}) was added to the mixture, which was extracted with DCM. The collected organic layer was dried over anhydrous magnesium sulfate. After solvent evaporation, the crude product was purified by a silica gel column using petroleum ether (60–90 °C)/ethyl acetate (10 : 1 by volume) as eluent. A white solid was obtained in 47% yield (0.8 g). ^{1}H NMR (400 MHz, DMSO-d_6, δ, ppm): 9.33 (s, 1H, OH), 7.05–7.14 (m, 9H), 6.91–6.97 (m, 6H), 6.72 (d, 2H), 6.50 (d, 2H). ^{13}C NMR (400 MHz, DMSO-d_6, δ): 156.4, 144.1, 141.0, 139.5, 134.1, 132.3, 131.1, 128.2, 126.6, 115.1.

Synthesis of *N*,*N*′-dicyclohexyl-1,7-di(4-(1,2,2-triphenyl)-vinyl)-phenoxyperylene-3,4:9,10-tetracarboxylic bisimide

Into a 250 mL two-necked round-bottom flask, the mixture of 1,6- and 1,7-DBrPBI (0.5 g, 0.7 mmol), 1-(4-hydroxyphenyl)-1,2,2-triphenylethene (0.85 g, 2.5 mmol), and K_2CO_3 (0.3 mg, 2.3 mmol) and NMP (35 mL) were added. The mixture was stirred overnight at 80 °C under N_2 atmosphere. After cooled to room temperature, the mixture was added to 80 mL dilute hydrochloric acid (1 M). The resulting precipitate was separated by filtration. The crude product was purified by a silica gel column using DCM as eluent. The latter main segment was collected and recrystallized from MeOH and chloroform for three times. A red solid was obtained in 64% yield (0.56 g). The characterization data indicated that the compound was pure *N*,*N*′-dicyclohexyl-1,7-di(4-(1,2,2-triphenyl)-vinyl)-phenoxy-perylene-3,4:9,10-tetracarboxylic bisimide (BTPEPBI). ^{1}H NMR (400 MHz, $CDCl_3$, δ, ppm): 9.41 (d, 2H), 8.52 (d, 2H), 8.21 (s, 2H), 7.19–7.23 (m, 4H), 7.04–7.15 (m, 30H), 6.86 (d, 4H), 5.03 (m, 2H), 2.58 (m, 4H) 1.95 (m, 4H), 1.77 (m, 6H), 1.50 (m, 4H) 1.37 (m, 2H); ^{13}C NMR (400 MHz, $CDCl_3$, δ, ppm): 163.7, 163.1, 154.9, 153.4, 143.5, 143.2, 141.5, 140.6, 139.7, 133.4, 132.9, 131.3129.9, 128.9, 128.6, 127.8, 126.6, 125.0, 124.3, 124.0, 123.6, 122.6, 118.6, 53.9, 29.0, 26.5, 25.4. Anal. calcd for $C_{88}H_{66}N_2O_6 \cdot H_2O$: C 83.52, H 5.42, N 2.21; found: C 83.24, H 5.43, N 2.32.

Synthesis of BTPEPBI-containing NPs

A THF solution (0.5 mL) containing 1 mg of BTPEPBI and 2 mg of the mixture of DSPE–PEG_{2000} and DSPE–PEG_{5000}–Folate (molar ratio of 1 : 0 and 1 : 1, respectively) was poured into 10 mL of 90% (v/v) water–THF solution. This was followed by sonicating the mixture for 60 s at 12 W output using a microtip probe sonicator (XL2000, Misonix Incorporated, NY). The emulsion was then stirred at room temperature overnight to evaporate THF. BTPEPBI-NP0 and BTPEPBI-NP50 are assigned to BTPEPBI based NPs prepared with 0% and 50% of the DSPE–PEG_{5000}–Folate at the feed. The obtained solution was filtered over a 0.22 μm syringe-driven filter to collect the products.

Cell culture

MCF-7 breast cancer cells and murine hepatic H_{22} cancer cells were cultured in folate-free Dulbecco's Modified Eagle Medium (DMEM) containing 10% fetal bovine serum and 1% penicillin streptomycin at 37 °C in a humidified environment containing 5% CO_2, respectively. Before experiment, the cells were pre-cultured until confluence was reached.

Cell imaging

MCF-7 breast cancer cells were cultured in the confocal imaging chambers (LAB-TEK, Chambered Coverglass System) at 37 °C.

View Article Online

Published on 28 May 2012. Downloaded by HK University of Science and Technology on 24/04/2014 05:13:22.

After 80% confluence, the medium was removed and the adherent cells were washed twice with 1× PBS buffer. The BTPEPBI-NP0 and BTPEPBI-NP50 in FBS-free DMEM medium at 2 μM of BTPEPBI were then added to the chambers, respectively. After incubation for 2 h, the cells were washed three times with 1× PBS buffer and then fixed by 75% ethanol for 20 minutes, which were further washed twice with 1× PBS buffer and stained by DAPI for 10 min. The cell monolayer was then washed twice with 1× PBS buffer and imaged by confocal laser scaning microscopy (CLSM, Zeiss LSM 410, Jena, Germany) with imaging software (Olympus Fluoview FV1000) under the same experimental conditions. The fluorescence signal from BTPEPBI-NPs was collected at 543 nm excitation with a 560 nm longpass barrier filter. The images were analyzed using Image-Pro Plus 5.0 software to obtain the average fluorescence intensity of red signal for MCF-7 cells.

In vivo fluorescence imaging

All animal experiments were performed in compliance with guidelines set by the Institutional Animal Care and Use Committee (IACUC), Singapore General Hospital. 0.1 mL of H_{22} cell suspension containing 5–6 × 10^6 cells were injected subcutaneously to ICR mice (average body weight of 25 g) at the left axilla. When the tumor volume reached a mean size of about 300 mm^3, the mice were intravenously injected with 250 μL of BTPEPBI-NP50 and BTPEPBI-NP0, respectively, at the dye concentration of 4 mg kg^{-1} animal. Subsequently, the mice were anesthetized and placed on an animal plate heated to 37 °C. The biodistribution in mice was imaged using the Maestro *in vivo* fluorescence imaging system (CRi, Inc.). The light with a central wavelength at 523 nm was selected as the excitation source. *In vivo* spectral imaging from 560 to 900 nm (10 nm step) was conducted with an exposure time of 150 ms for each image frame. Auto-fluorescence was removed by using the spectral unmixing software. Scans were carried out at 1 h and 3 h post-injection.

Acknowledgements

This work was supported by the National Science Foundation of China (21074113); the key project of the Ministry of Sci. & Technol. of China (2009CB623605), the Science Foundation of Zhejiang Province (Z4110056), the Research Grants Council of Hong Kong (603509, HKUST2/CRF/10, and 604711), the SRFI grant of HKUST (SRFI11SC03PG), the NSFC/RGC grant (N_HKUST620/11), the University Grants Committee of Hong Kong (AoE/P-03/08), the National Research Foundation of Singapore (R279-000-323-281) and the Institute of Materials Research and Engineering of Singapore (IMRE/11-1C0213). B.Z.T. thanks the support from the Cao Guangbiao Foundation of Zhejiang University.

Notes and references

1 (*a*) R. H. Newman, M. D. Fosbrink and J. Zhang, *Chem. Rev.*, 2011, **111**, 3614–3666; (*b*) H. Kobayashi, M. Ogawa, R. Alford, P. L. Choyke and Y. Urano, *Chem. Rev.*, 2010, **110**, 2620–2640; (*c*) M. Sameiro and T. Gonçalves, *Chem. Rev.*, 2009, **109**, 190–212; (*d*) S. W. Thomas III, G. D. Joly and T. M. Swager, *Chem. Rev.*, 2007, **107**, 1339–1386.

2 (*a*) M. B. Borgia1, A. Borgia, R. B. Best, A. Steward, D. Nettels, B. Wunderlich, B. Schuler and J. Clarke, *Nature*, 2011, **474**, 662–666; (*b*) A. C. Meinema, J. K. Laba, R. A. Hapsari, R. Otten, F. A. A. Mulder, A. Kralt, G. van den Bogaart, C. P. Lusk, B. Poolman and L. M. Veenhoff, *Science*, 2011, **333**, 90–93; (*c*) C. A. Traina, R. C. Bakus II and G. C. Bazan, *J. Am. Chem. Soc.*, 2011, **133**, 12600–12607; (*d*) A. Duarte, A. Chworos, S. V. Flagan, G. Hanrahan and G. C. Bazan, *J. Am. Chem. Soc.*, 2010, **132**, 12562–12564.

3 (*a*) C. Allain, S. R. Lartia, G. Bordeau, F. D. F. Charra, P. Tauc and M. Teulade-Fichou, *ChemBioChem*, 2007, **8**, 424–433; (*b*) X. Shu, A. Royant, M. Z. Lin, T. A. Aguilera, V. LevRam, P. A. Steinbach and R. Y. Tsien, *Science*, 2009, **324**, 804–807; (*c*) B. Zhu, H. Jia, X. Zhang, Y. Chen, H. Liu and W. Tan, *Anal. Bioanal. Chem.*, 2010, **397**, 1245–1250; (*d*) T. Egawa, Y. Koide, K. Hanaoka, T. Komatsu, T. Terai and T. Nagano, *Chem. Commun.*, 2011, **47**, 4162–4164; (*e*) Y. Koide, Y. Urano, K. Hanaoka, T. Terai and T. Nagano, *J. Am. Chem. Soc.*, 2011, **133**, 5680–5682; (*f*) T. Cheng, T. Wang, W. Zhu, X. Chen, Y. Yang, Y. Xu and X. Qian, *Org. Lett.*, 2011, **13**, 3656–3659.

4 (*a*) H. Imahori, T. Umeyama and S. Ito, *Acc. Chem. Res.*, 2009, **42**, 1809–1818; (*b*) J.-L. Brédas, J. E. Norton, J. Cornil and V. Coropceanu, *Acc. Chem. Res.*, 2009, **42**, 1691–1699.

5 (*a*) F. J. M. Hoeben, P. Jonkheijm, E. W. Meijer and A. P. H. J. Schenning, *Chem. Rev.*, 2005, **105**, 1491–1684; (*b*) K. Balakrishnan, A. Datar, R. Oitker, H. Chen, J. Zuo and L. Zang, *J. Am. Chem. Soc.*, 2005, **127**, 10496–10497; (*c*) Z. J. Ning, Z. Chen, Q. Zhang, Y. L. Yan, S. X. Qian, Y. Cao and H. Tian, *Adv. Funct. Mater.*, 2007, **17**, 3799–3807.

6 (*a*) F. Würthner, *Chem. Commun.*, 2004, 1564–1579; (*b*) Z. Chen, U. Baumeister, C. Tschierske and F. Würthner, *Chem.–Eur. J.*, 2007, **13**, 450–465; (*c*) C. Huang, S. Barlow and S. R. J. Marder, *J. Org. Chem.*, 2011, **76**, 2386–2407.

7 (*a*) M. R. Wasielewski, *Acc. Chem. Res.*, 2009, **42**, 1910–1921; (*b*) R. F. Kelley, W. S. Shin, B. Rybtchinski, L. E. Sinks and M. R. Wasielewski, *J. Am. Chem. Soc.*, 2007, **129**, 3173–3181; (*c*) H. Yoo, J. Yang, A. Yousef, M. R. Wasielewski and D. Kim, *J. Am. Chem. Soc.*, 2010, **132**, 3939–3944.

8 (*a*) M. Franceschin, N. Borbone and G. Oliviero, *Bioconjugate Chem.*, 2011, **22**, 1309–1319; (*b*) A. Fercher, S. M. Borisov, A. V. Zhdanov, I. Klimant and D. B. Papkovsky, *ACS Nano*, 2011, **5**, 5499–5508; (*c*) H. Bittermann, D. Siegemund, V. L. Malinovskii and R. Haner, *J. Am. Chem. Soc.*, 2008, **130**, 15285–15287.

9 (*a*) L. C. Palmer and S. I. Stupp, *Acc. Chem. Res.*, 2008, **41**, 1674–1684; (*b*) H. Usta, A. Facchetti and T. J. Marks, *Acc. Chem. Res.*, 2011, **44**, 501–510; (*c*) L. Zang, Y. Che and J. S. Moore, *Acc. Chem. Res.*, 2008, **41**, 1596–1608.

10 (*a*) K. Balakrishnan, A. Datar, T. Naddo, J. Huang, R. Oitker, M. Yen, J. Zhao and L. Zang, *J. Am. Chem. Soc.*, 2006, **128**, 7390–7398; (*b*) X.-Q. Li, X. Zhang, S. Ghosh and F. Würthner, *Chem.–Eur. J.*, 2008, **14**, 8074–8078; (*c*) S. Ghosh, X. Q. Li, V. Stepanenko and F. Würthner, *Chem.–Eur. J.*, 2008, **14**, 11343–11357.

11 (*a*) Y. Che, X. Yang, K. Balakrishnan, J. Zuo and L. Zang, *Chem. Mater.*, 2009, **21**, 2930–2934; (*b*) M. K. R. Fischer, T. E. Kaiser, F. Würthner and P. Bauerle, *J. Mater. Chem.*, 2009, **19**, 1129–1141; (*c*) J. Qu, J. Zhang, A. C. Grimsdale, K. Müllen, F. Jaiser, X. Yang and D. Neher, *Macromolecules*, 2004, **37**, 8297–8306.

12 (*a*) J. Luo, Z. Xie, J. W. Y. Lam, L. Cheng, H. Chen, C. Qiu, H. S. Kwok, X. Zhan, Y. Liu, D. Zhu and B. Z. Tang, *Chem. Commun.*, 2001, 1740–1471; (*b*) B. K. An, S. K. Kwon, S. D. Jung and S. Y. Park, *J. Am. Chem. Soc.*, 2002, **124**, 14410–14415; (*c*) Y. N. Hong, J. W. Y. Lam and B. Z. Tang, *Chem. Commun.*, 2009, 4332–4353; (*d*) Y. N. Hong, J. W. Y. Lam and B. Z. Tang, *Chem. Soc. Rev.*, 2011, **40**, 5361–5388.

13 (*a*) Z. J. Zhao, P. Lu, J. W. Y. Lam, Z. M. Wang, C. Y. K. Chan, H. H. Y. Sung, I. D. Williams, Y. G. Ma and B. Z. Tang, *Chem. Sci.*, 2011, **2**, 672–675; (*b*) Z. J. Zhao, S. M. Chen, J. W. Y. Lam, Z. M. Wang, P. Lu, F. Mahtab, H. H. Y. Sung, I. D. Williams, Y. G. Ma, H. S. Kwok and B. Z. Tang, *J. Mater. Chem.*, 2011, **21**, 7210–7216; (*c*) Z. Zhao, S. Chen, J. W. Y. Lam, P. Lu, Y. Zhong, K. S. Wong, H. S. Kwok and B. Z. Tang, *Chem. Commun.*, 2010, **46**, 2221–2223; (*d*) W. Z. Yuan, P. Lu, S. Chen, J. W. Y. Lam, Z. Wang, Y. Liu, H. S. Kowk, Y. Ma and B. Z. Tang, *Adv. Mater.*, 2010, **22**, 2159–2163.

 This journal is © The Royal Society of Chemistry 2012

View Article Online

Published on 28 May 2012. Downloaded by HK University of Science and Technology on 24/04/2014 05:13:22.

14 B. A. Jones, M. J. Ahrens, M. H. Yoon, A. Facchetti, T. J. Marks and M. R. Wasielewski, *Angew. Chem., Int. Ed.*, 2004, **43**, 6363–6366.
15 (*a*) F. Würthner, V. Stepanenko, Z. Chen, C. R. Saha-Moller, N. Kocher and D. Stalke, *J. Org. Chem.*, 2004, **69**, 7933–7939; (*b*) L. Fan, Y. Xu and H. Tian, *Tetrahedron Lett.*, 2005, **46**, 4443–4447; (*c*) R. K. Dubey, A. Efimov and H. Lemmetyinen, *Chem. Mater.*, 2010, **23**, 778–788; (*d*) N. V. Handa, K. D. Mendoza and L. D. Shirtcliff, *Org. Lett.*, 2011, **13**, 4724–4727; (*e*) Q. Zhao, S. Zhang, Y. Liu, J. Mei, S. Chen, P. Lu, A. Qin, Y. Ma, J. Z. Sun and B. Z. Tang, *J. Mater. Chem.*, 2012, **22**, 7387–7394.
16 (*a*) D. Gonzalez-Rodriguez and A. P. H. J. Schenning, *Chem. Mater.*, 2011, **23**, 310–325; (*b*) T. F. A. De Greef, M. M. J. Smulders, M. Wolffs, A. P. H. J. Schenning, R. P. Sijbesma and E. W. Meijer, *Chem. Rev.*, 2009, **109**, 5687–5754; (*c*) J. E. Bullock, R. Carmieli, S. M. Mickley, J. Vura-Weis and M. R. Wasielewski, *J. Am. Chem. Soc.*, 2009, **131**, 11919–11929; (*d*) L. Zang, Y. Che and J. S. Moore, *Acc. Chem. Res.*, 2008, **41**, 1596–1608.
17 (*a*) C. Prashant, M. Dipak, C. T. Yang, K. H. Chuang, D. Jun and S. S. Feng, *Biomaterials*, 2010, **31**, 5588–5597; (*b*) K. Li, Y. Jiang, D. Ding, X. Zhang, Y. Liu, J. Hua, S.-S. Feng and B. Liu, *Chem. Commun.*, 2011, **47**, 7323–7325.
18 (*a*) V. Dixit, J. V. Bossche, D. M. Sherman, D. H. Thompson and R. P. Andres, *Bioconjugate Chem.*, 2006, **17**, 603–609; (*b*) J. Sudimack, D. H. Lee and R. J. Adv, *Adv. Drug Delivery Rev.*, 2000, **41**, 147–162.
19 P. S. Low, W. A. Henne and D. D. Doorneweerd, *Acc. Chem. Res.*, 2008, **41**, 120–129.
20 Z. Liu, K. Chen, C. Davis, S. Sherlock, Q. Cao, X. Y. Chen and H. J. Dai, *Cancer Res.*, 2008, **68**, 6652–6660.
21 S. D. Li and L. Huang, *Mol. Pharmaceutics*, 2008, **5**, 496–504.